Available online at www.sciencedirect.com
SCIENCE DIRECT®
Polymer 44 (2003) 3491–3508
polymer
www.elsevier.com/locate/polymer

Influence of fractionated crystallization on the semicrystalline structure of (POM/(PS/PPE)) blends. Static and time-resolved SAXS, WAXD and DSC studies

V. Everaert[a], G. Groeninckx[a,*], M.H.J. Koch[b], H. Reynaers[a]

[a]*Department of Chemistry, Laboratory for Macromolecular Structural Chemistry, Catholic University of Leuven, Celestijnenlaan 200F, B-3001 Heverlee, Belgium*
[b]*European Molecular Biology Laboratory, Hamburg Outstation, EMBL c/o DESY, Notkestrasse 85, D-22603 Hamburg, Germany*

Received 15 July 2002; received in revised form 24 February 2003; accepted 18 March 2003

Abstract

The semicrystalline structure and degree of crystallinity of fractionated crystallizing poly(methylene oxide)/(polystyrene/poly(2,6-dimethyl-1,4 phenylene ether) POM/(PS/PPE) blends have been investigated by DSC, SAXS and WAXD. The three techniques yielded highly correlated results.

The degree of crystallinity of the POM phase determined by DSC ($X_{c,DSC}$) decreases with decreasing POM content in the blends and this is accompanied by a shift from bulk to homogeneous crystallization.

The reduction in the measured degree of crystallinity determined by WAXD ($X_{c,WAXD}$) is even more pronounced and indicates, in absence of evidence for the formation of different polymorphs, that only small and imperfect crystals are formed during homogeneous crystallization in finely dispersed droplets. Analysis of the width of the WAXD reflections, which is also related to $X_{c,WAXD}$, yields a linear correlation between L_1, a measure of the lateral dimensions of the crystallites, and the average dispersed particle diameter. The parameter L_2, corresponding to the crystalline lamellar thickness, is non-linearly correlated with the degree of crystallinity, indicating that the decrease in $X_{c,WAXD}$ is not solely due to the formation of thinner lamellae at higher degrees of undercooling. There is a simple relationship between the SAXS long period and the crystallization temperature, corresponding to the formation of thinner and less perfect crystalline lamellae during fractionated crystallization at higher degrees of undercooling.

As the lateral dimensions of the crystallites of finely dispersed crystallizing droplets is governed by their size, $X_{c,WAXD}$ can be directly related to the particle diameter, since the fraction of small or imperfect crystallites will not be measured by WAXD.
© 2003 Elsevier Science Ltd. All rights reserved.

Keywords: Poly(methylene oxide)/(polystyrene/poly(2,6-dimethyl-1,4 phenylene ether blends; Fractionated crystallization; Semicrystalline structure

1. Introduction

Binary mixtures of immiscible polymers, where one of the components is in excess, usually display a typical droplet-in-matrix phase morphology. The size of the dispersed particles depends on the blend composition, melt-viscosity and elasticity of each phase, interfacial tension and mixing conditions [1–3]. When the dispersed phase component can crystallize, the particle size has a crucial impact on its crystallization behavior, due to fractionated crystallization [4]. This phenomenon has been investigated for several immiscible polymer blend systems: HDPE/POM [5], PVDF/PA-6 [6,7], PVDF/PBT [6,7], PVDF/PA-66 [8], EPDM/PA-6 [9], PS/iPP [10], PS/LDPE [11], PS/LLDPE [12,13], LLDPE/iPP [13], SBR/iPP [14], PS/PEG [15], iPP/PEG [16], and iPP/PA-6 [17,18].

Fractionated crystallization can be considered as a sequence of primary nucleation steps at increasing degrees of undercooling, ΔT_c, often culminating in massive crystallization at the homogeneous nucleation temperature, $T_{c,hom}$ [7,10,11,14]. The phenomenon was related to the size of the dispersed droplets, by following the amount of solidified polymeric droplets suspended in an inert liquid medium by optical microscopy [4,19]. A theoretical analysis [7] relates

* Corresponding author. Tel.: +32-1632-7441; fax: +32-1632-7779.
E-mail address: gabriel.groeninckx@chem.kuleuven.ac.be (G. Groeninckx).

0032-3861/03/$ - see front matter © 2003 Elsevier Science Ltd. All rights reserved.
doi:10.1016/S0032-3861(03)00254-4

each fraction that crystallizes upon cooling from the melt to primary nucleation from heterogeneities with different specific interfacial energy differences (Δy_i) between the polymeric chain and the nucleating substrate. Usually, only the heterogeneities with the smallest Δy-value are efficient in primary nucleation. Crystallization subsequently extends in the bulk to the whole volume by secondary nucleation, and is complete before the undercooling, $\Delta T_{c,2}$, of the next Δy-class of heterogeneities is reached.

If the minor phase component is dispersed in numerous droplets, each of these will start crystallizing from its own lowest Δy heterogeneities. The number of dispersed droplets often exceeds the number of heterogeneities promoting crystallization near the bulk crystallization temperature. Consequently, small droplets that have a lower probability of containing such nucleation centers will start crystallizing from other types of heterogeneities at much higher degrees of undercooling, or even homogeneously crystallize by self-association of the polymer chains.

Fractionated crystallization is often accompanied by a large drop in X_c of the dispersed phase. For the dispersed PP phase in PP/PS blends the enthalpy of crystallization, ΔH_c, drops from 95 J/g in pure bulk crystallized PP to 75 J/g in the fully homogeneously crystallizing PP/PS 10/90 blend [10]. Addition of 1 wt% phthalocyanine blue, which is a powerful nucleating agent for PP, shifts the crystallization temperature far above the bulk nucleation temperature, but also increases the degree of crystallinity. Self-seeding experiments lead to the same result. Similarly, in PP/thermoplastic rubber blends (PP/TR), ΔH_c was reduced from 98.5 J/g in pure PP to 61 J/g in a PP/TR 25/75 blend [14]. In PS/HDPE blends with a finely dispersed HDPE phase the drop in X_c of HDPE from 80% in the homopolymer to 55% in the PS/HDPE 95/5 blend [20] was attributed to the change in crystallization temperature. An identical behavior was found for block copolymers with PEO as crystallizable component and attributed to the peculiar fractionated crystallization process of block copolymers due to the formation of microdomains with a size determined by the crystallizable chain length in the block copolymer, free from heterogeneous nuclei [21]. In block copolymers of PEO–PI–PEO with a minor amount of PEO the drop in X_c from 96% in the homopolymer to 69% in the block copolymer is accompanied by a melting point depression [22]. A decrease in X_c of the microdomain phase and a melting point depression, both attributed to the formation of less perfect crystalline lamellae in the microdomains [15], were also observed for PEO–PI, PEO–PS–PEO [20], and PEMA–PEO [23]. In PVDF/PA-6 blends however, no change in X_c of the dispersed phase could be observed as a consequence of the mutual nucleating ability of both components [6]. This suggests that the decrease of X_c in fractionated crystallizing blends cannot solely be attributed to the formation of thinner and less perfect crystalline structures at higher degrees of undercooling, as generally assumed [7].

A survey of the literature confirms that fractionated crystallization can have a non-negligible impact on both the degree of crystallinity and the morphology (i.e. lamellar thickness, long spacing and crystal perfection). These parameters are of crucial importance for the thermal and mechanical properties of the blends [24].

In this study, the fractionated crystallization in immiscible blends of POM dispersed in an amorphous miscible PS/PPE matrix has been investigated. This model system allows to vary both the melt-viscosity ratio of the blend system, hence creating different blend phase morphologies, and the physical state of the amorphous matrix during crystallization of the dispersed POM droplets (Fig.1).

In previous work [25], no clear relationship could be established between the degree of crystallinity obtained by DSC and the blend phase morphology. Since it is likely that the degree of crystallinity would be governed by the semicrystalline structure, which in turn depends on the crystallization conditions and thermal history, the micro-morphological characteristics of the POM phase in the blends was studied by simultaneous SAXS–WAXD. The influence of blend phase morphology, physical state of the matrix phase, and crystallization conditions (i.e. temperature, cooling rate, thermal history) on the semicrystalline structure of the dispersed POM phase were investigated.

2. Experimental

2.1. Materials

The characteristics of the materials used in this study are listed in Table 1. POM is a commercial grade Celcon® M-50 POM copolymer (Celanese, USA) containing about 5 wt% ethylene oxide as stabilizer against thermal degradation; its melting point is 175 °C. PS is a commercial grade Styron® E680 (Dow Benelux N.V., Terneuzen, NL) with $T_g = 102$ °C. PPE is a PPE-800 grade supplied by General Electric Plastics (Bergen-op-Zoom, NL) with $T_g = 215$ °C.

2.2. Miscible amorphous PS/PPE phases

The amorphous phases were prepared by melt-blending

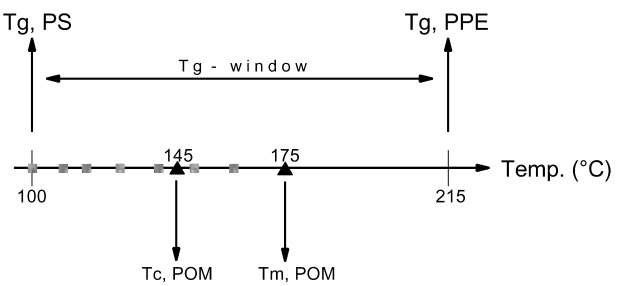

Fig. 1. Schematical representation of the POM/(PS/PPE) model blend system. The T_g of the miscible amorphous PS/PPE phase can be varied around T_c or T_m of the crystallizable POM phase.

Table 1
Basic material characteristics

Material	MFI (g/10 min)	M_n (GPC)	M_w (GPC)	Polydispersity	Density (g/cm^3)
POM	–		± 70,000		1.4
PS	–	81,900[a]	190,000[a]	2.6	1.055
PPE	13 (300 °C)	19,300[a]	54,300[a]	2.8	1.065

[a] Measured in THF at 25 °C; molecular weights are based on polystyrene standards.

PS and PPE which are perfectly miscible over the whole composition range [26,27]. Both the melt-viscosity and the glass transition temperature of the amorphous phase can thus be varied without altering the interfacial tension between POM and these miscible amorphous components [28]. Blending was performed in a Haake Rheocord 90 twin screw extruder at 285 °C with a screw speed of 120 rpm, after drying the materials for at least one night at 40 °C under vacuum. The homogeneity of each blend was verified by DSC.

For the present study, two PS/PPE compounds were selected as representative examples for the low viscosity/-low viscosity (LL) and low viscosity/high viscosity (LH) blends discussed previously [25]. The PS/PPE 85/15 compound with $T_g = 114$ °C and melt-viscosity at 260 °C and 50 s^{-1} of 323 Pa s, referred to as Ha4, has a viscosity ratio with POM of 1.56 and is representative for the LL blends. The PS/PPE 50/50 compound with $T_g = 144$ °C and melt-viscosity at 260 °C and 50 s^{-1} of 2068 Pa s, referred to as Ha7, has a viscosity ratio with POM of 0.25 and is representative for the LH blends.

2.3. Compounding of the POM/(PS/PPE) blends

All materials were melt-blended under nitrogen in a mini-extruder (DSM Research, Geleen, NL), which is a conical co-rotating fully intermeshing twin-screw extruder, with a capacity of about 4 cm^3. Mixing during 5 min at 260 °C at a screw speed of 50 rpm resulted in a well dispersed phase morphology for both low and high viscosity materials. After blending, the melt was immediately quenched at the die exit in an isopropanol/solid CO_2 mixture.

POM/(PS/PPE) blends were prepared for both POM/Ha4 and POM/Ha7 systems in a wt% blend compositions of 60/40, 40/60, 30/70, 20/80, 15/85, 10/90 and 5/95.

2.4. Morphological analysis

To correlate the crystallization behaviour and the semicrystalline structure of POM in the POM/(PS/PPE) blends with the blend phase morphology, all samples were subjected to the same thermal program as used during the DSC measurements, prior to phase morphology analysis. Extruded strands were therefore thermally treated in a Mettler hot-stage. Procedures used for the visualisation and analysis of the blend phase morphology have been described elsewhere [25].

2.5. Thermal analysis of the blends

DSC measurements on the blends were performed on a Perkin Elmer Delta series DSC7, calibrated with indium ($T_m = 156$ °C) and benzophenone ($T_m = 48$ °C). Samples were first heated at 10 °C/min to a melt temperature of 200 °C, and kept there for 2 min to erase the thermal history. Subsequently, they were cooled at 10 °C/min to 50 °C and the dynamic crystallization behaviour was recorded. Heating from 80 to 200 °C at 10 °C/min allowed to assess the corresponding melting characteristics of blends crystallized in a controlled manner.

2.6. Static WAXD experiments

Static WAXD measurements at room temperature were made a horizontal Geigerflex diffractometer installed on a Rigaku Rotaflex Ru-200B rotating anode operated at 40 kV and 100 mA. Samples of 1 mm thickness were prepared by compression molding at 210 °C and subsequently cooled in a Mettler hot stage under conditions simulating the thermal treatment performed in DSC. WAXD patterns were recorded in transmission mode in 0.05° steps between $5° < 2\theta < 39°$ (2θ is the scattering angle) with measuring periods between 10 and 30 s. The background scattering corresponding to an empty sample holder was subtracted from the experimental curves.

The degree of crystallinity ($X_{c,WAXD} = (S_{100} + S_{105})/(S_{100} + S_{105} + S_a)$) was estimated from the ratio of the area of the diffraction pattern under the (100) reflection (S_{100}) and the (105) reflection (S_{105}) to the total area under the normalized WAXD curve including that under the amorphous halo (S_a) [29–31]. The amorphous halo was fitted using a Lorentzian and the (100) and (105)-reflections with a Pearson function using the Origin 5.0 Peak-fitting software package (Microcal Software Inc., USA).The crystallite sizes in the POM phase were estimated on a relative scale with the Scherrer equation (Eq. 1), relating crystallite dimensions to the width of the reflections [32,33].

$$L = \frac{0.9\lambda}{(\Delta B - \Delta B_0)\cos\theta} \quad (1)$$

In this expression, L is the crystallite size perpendicular to the reflecting plane, λ is the wavelength, 2θ is the scattering angle of the diffraction peak, ΔB is the observed peak width at half-maximum intensity, and ΔB_0 the instrumental line width, which depends on the sample thickness, wavelength and collimation.

2.7. Real-time SAXS and WAXD experiments

Time-resolved simultaneous SAXS/WAXS synchrotron

radiation experiments were carried out on the double focussing X33 beam line ($\lambda = 0.15$ nm) of the EMBL in HASYLAB on the storage ring DORIS III of the Deutsches Elektronen Synchrotron (DESY) at Hamburg [34–36] using two gas proportional detectors connected in series [37]. Samples with a thickness of 1 mm were sealed between thin aluminum foils and mounted in a Mettler hot stage placed in the X-ray beam path, and submitted to the same thermal treatment as in DSC. The scattering vector axis ($s = 2 \times \sin \vartheta/\lambda$, with 2ϑ the scattering angle and λ the wavelength) of the SAXS region was calibrated using dry collagen, and that of the WAXD region with a standard polyethylene sample or tripalmitin. The experimental curves collected in 6 s time frames were normalized to the intensity of the primary beam monitored with an ionization chamber.

The scattering corresponding to an amorphous sample in the molten state was subtracted from the experimental SAXS curves. Linear correlation functions [38], where calculated assuming an ideal two-phase system [39] following standard procedures involving extrapolation of the patterns large s-values using Porod's law [40]. The normalization of the correlation function was performed by dividing by the invariant, Q [39]. The long period, $\langle L \rangle_n$, was found from the first side maximum in the correlation function. The volume degree of crystallinity within the lamellar stacks, ϕ, was determined from the quadratic expression. The amorphous or crystalline layer thickness, L_a or L_c, were calculated from the minimum in the correlation function and the tangent to the auto-correlation triangle.

For the analysis of the WAXD patterns, a relative crystallinity index was calculated from the evolution of the area under the (100)-reflection after subtraction of a linear background as a function of temperature.

3. Results and discussion

3.1. Overview of the blend morphology and the crystallization behavior

The fractionated crystallization behavior of POM/-(PS/PPE) blend system has been reported previously [25]. Two main types of blends can be distinguished on the basis of the viscosity ratio, p, (i.e. the ratio of the viscosity of the dispersed POM phase (η_d) to that of the PS/PPE matrix (η_m)): low viscosity/low viscosity (LL) blends with $p \geq 1$ (represented by POM/Ha4 blends) and low viscosity/high viscosity (LH) blends with $p \ll 1$ (represented by POM/Ha7 blends). The crystallization behavior of the investigated blends as a function of POM content is illustrated in Fig. 2.

LL blends display an equilibrium blend phase morphology after melt-mixing and subsequent thermal treatment simulating a DSC run. There is a narrow region of phase inversion around the 50/50 composition and blends containing minor amounts of POM always form a clear dispersion of POM droplets in a PS/PPE matrix with a rather broad particle size distribution. The DSC scans during cooling from the melt in such blends typically exhibit multiple crystallization peaks and bulk crystallized material completely disappears as soon as POM forms the dispersed phase.

For LH blends, no equilibrium phase morphology could develop in the region of phase inversion, which is broad and characterized by a complex composite-like phase morphology consisting of co-continuous POM and PS/PPE phases and small POM subinclusions in the PS/PPE domains. Outside this region, very small POM droplets with a narrow size distribution are found. The crystallization behavior in this blend series is strongly influenced by the phase morphology and displays some additional bulk crystallization, which is probably related to the vitrified state of the PS/PPE phase at T_c [25].

The degree of crystallinity in both blend series significantly drops as the content of POM decreases, i.e. when a larger fraction of material crystallizes at higher degrees of undercooling (Fig. 2b).

Several factors must be taken into account to explain the effect of fractionated crystallization on the semicrystalline structure and crystallinity:

(i) *Errors in $\Delta H_{c,POM}$ from DSC due to normalization procedures*. The degree of crystallinity of the POM phase determined by DSC is obtained by normalizing the total crystallization enthalpy to the amount of POM in the blend. This introduces two sources of error: (a) The exact amount of POM phase in a 5 mg sample may not exactly correspond to the original preset blend composition due to local inhomogeneities in the morphology leading to an over- or underestimate of the actual degree of crystallinity. (b) For similar reasons, normalization of the total crystallization enthalpy to the POM fraction in the blend will be less accurate at lower POM contents.

(ii) *Formation of different polymorphic forms*. POM exists in a trigonal form obtained under normal crystallization conditions or in an orthorhombic form [41]. Because homogeneously crystallized samples are subject to different crystallization conditions, the nature of the crystalline phase after homogeneous crystallization must be established.

(iii) *Formation of thinner and/or less perfect crystalline lamellae*. Crystallization at higher degrees of undercooling occurs at different growth rates, G, which reach a maximum between T_g (mobility restrictions) and T_m (nucleation restrictions). The temperature corresponding to the maximum growth rate can be estimated from a single mastercurve with a reduced temperature scale $(T - T_g + 50)/(T_m - T_g + 50)$ [42] where G_{max} corresponds to a reduced temperature of 0.6. For the POM copolymer ($T_m \approx 175$ °C; $T_g \approx -55$ °C) and G_{max} must be situated around 63 °C. The homogeneous crystallization temperature of POM is around 91 °C

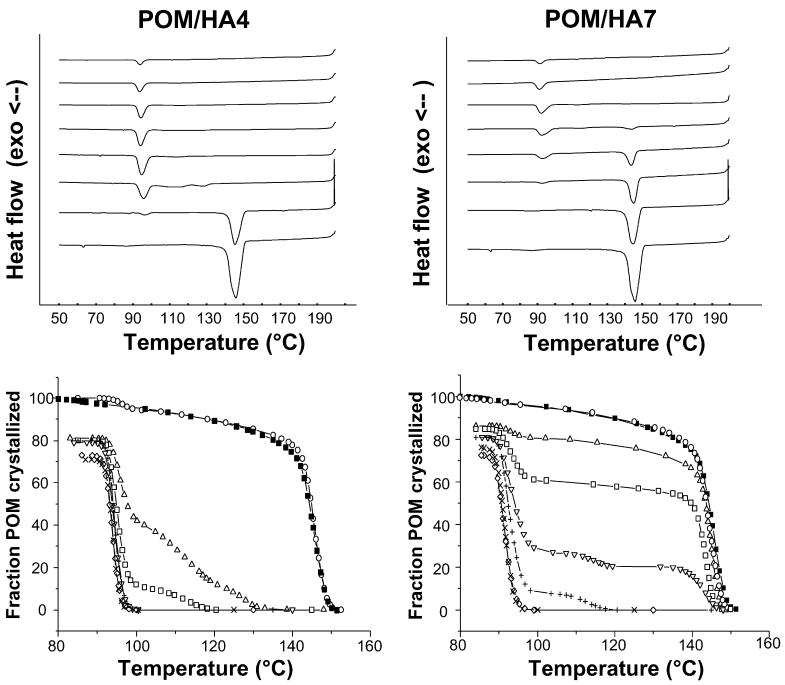

Fig. 2. Dynamic crystallization behavior as measured by DSC in POM/Ha4 and POM/Ha7 blends. Dynamic DSC traces and corresponding integrated DSC curves normalized to the degree of crystallinity for pure POM (■), and POM/(PS/PPE) 60/40 (○), 40/60 (△), 30/70 (□), 20/80 (▽), 15/85 (+), 10/90 (◇) and 5/95 (×).

and it can be assumed that the linear growth rate of the spherulites steadily increases with increasing degree of undercooling. As long as mobility is not restrictive, higher crystallization rates are expected to give rise to thinner and/or less perfect crystalline lamellae, resulting in a lower degree of crystallinity [43,45].

(iv) *Non-spherulitic semicrystalline structure*. Droplets may not always be able to crystallize homogeneously in a spherulitic morphology. In the POM/Ha7 blends, for example droplets sometimes have diameters as small as 0.28 μm and confinement may thus play an important role in the development of the semicrystalline structure.

(v) *Non-crystallized small droplets*.

Finally, it is questionable that all droplets could crystallize during dynamic crystallization at a constant cooling rate of 10 °C/min. Due to volume limitations, smaller droplets will crystallize more slowly than a larger sample obeying the Evans–Avrami law [46]. The smaller the nodule, the slower the transformation and the lower the crystallization temperature [47]. If the crystallization kinetics becomes slower than the imposed cooling rate the smallest droplets may not or only partially crystallize, causing the DSC degree of crystallinity to decrease.

To find an answer to these questions, the results of simultaneous SAXS /WAXD experiments were compared with those of DSC. WAXD can be used to determine the polymorphs formed during fractionated crystallization and to estimate the degree of crystallinity and crystallite size. SAXS can provide information on the semicrystalline structure on a lamellar scale during the course of crystallization. The possibility that some of the smallest droplets would no longer be able to crystallize can be rejected since cold crystallization is not observed during subsequent heating and the rate of homogeneous nucleation is generally extremely high [25,44,48].

3.2. Static wide angle X-ray diffraction measurements

In order to determine the degree of crystallinity and the possible formation of different polymorphic forms, static WAXD measurements were performed on dynamically crystallized POM/Ha4 and POM/Ha7 samples. By keeping all parameters of the measurement constant, absolute measurements could be performed, both for the POM/Ha blends and the homogeneous PS/PPE compounds. Since the POM/(PS/PPE) blend system is completely immiscible, the WAXD pattern obtained is the superposition of that of the amorphous PS/PPE phase and of the semicrystalline POM phase. The amorphous PS/PPE halo was scaled to the pattern of the blend sample in the range $5° < 2\theta < 7°$ where POM gives rise neither to an amorphous halo nor to crystalline diffraction peaks. Subtraction of these scaled patterns yields that of the POM phase in the blend, from which the degree of crystallinity, $X_{c,WAXD}$, and crystallite size (Eq. 1) can be calculated. Examples of this calculation for both blend series are given in Fig. 3.

The original diffraction patterns and those obtained after

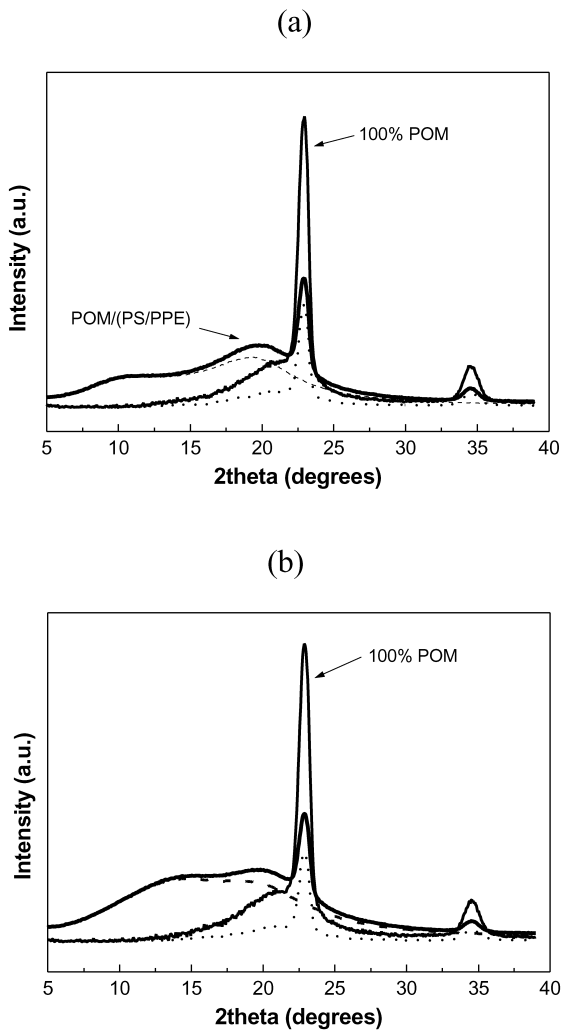

Fig. 3. Processing method of WAXD patterns of immiscible POM/(PS/PPE) blends. The measured WAXD spectrum of the blend (full bold line) and the WAXD spectrum of the pure amorphous phase (dashed line) are fitted onto each other in the 5–7° 2θ region. The result after subtraction (dotted line) can be considered as the WAXD pattern of the POM phase solely, and is normalized to 100% POM (full fine line). (a) a POM/Ha4 blend; (b) a POM/Ha7 blend.

subtraction of the amorphous PS/PPE phase are presented in Fig. 4. The two reflections correspond to the (100) lattice plane ($d = 3.88$ Å) parallel to the molecular axes and the (105) lattice plane ($d = 2.60$ Å). The amorphous halo of POM has a maximum at a spacing of 4.25 Å.

Only the trigonal (hexagonal) polymorph is formed during fractionated crystallization and the bulk and homogeneously crystallized blend samples display two reflexions at the same spacings as in pure POM. Furthermore, the intensity of the crystalline reflections is significantly reduced with decreasing content of POM, which is in agreement with the expected reduction in X_c. The results of a quantitative evaluation of $X_{c,WAXD}$ are shown in Fig. 5.

For both blend series $X_{c,WAXD}$ decreases with decreasing POM contents. The reduction of $X_{c,WAXD}$ in POM/Ha7 blends is seen from 20 wt% POM onwards, while in

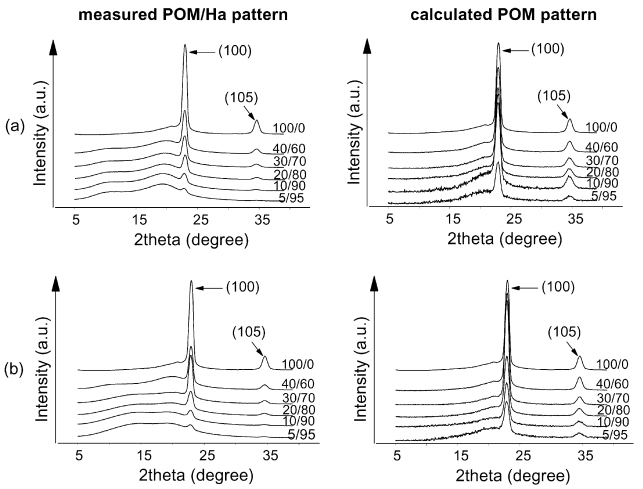

Fig. 4. Original WAXD spectra and the corresponding normalized 100% POM WAXD patterns for (a) POM/Ha4 blends and (b) POM/Ha7 blends.

POM/Ha4 blends, it is already observed from the 40/60 blend composition onwards. Table 2 illustrates that the drop in $X_{c,WAXD}$ in both blend series corresponds to the offset blend composition of the phase inversion region. As long as there is a co-continuous POM phase in the blend, heterogeneous nucleation at low degrees of undercooling can induce a normal crystallization. As soon as the blend phase morphology corresponds to fully dispersed POM droplets in a PS/PPE matrix $X_{c,WAXD}$ decreases. At low POM contents (≤ 20 wt% POM), $X_{c,WAXD}$ is nearly the same for both blend series, independently of the droplet size or percentage POM crystallized at higher degrees of undercooling.

There are substantial differences between the values of X_c obtained by DSC and WAXD, listed in Table 2,especially in POM/(PS/PPE) blends with low POM contents (< 10 wt% POM). Although these blends all exhibit the same degree of crystallinity in DSC and the same crystallization temperature, $X_{c,WAXD}$ further decreases. There is, however, no simple correlation between the fraction of POM crystallized at higher degrees of undercooling and $X_{c,WAXD}$. This suggests that the further

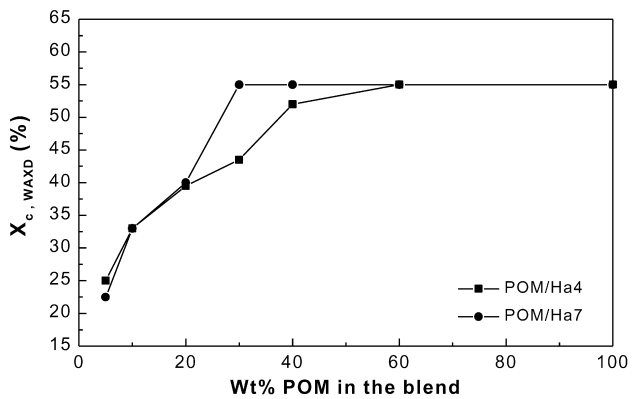

Fig. 5. Influence of the weight percentage POM in POM/(PS/PPE) blends on the degree of crystallinity, as measured from WAXD.

Table 2
Comparison of the degree of crystallinity determined by DSC ($X_{c,DSC}$) and WAXD ($X_{c,WAXD}$), in relation with morphological parameters and crystallization behavior

Material	DSC						WAXD	Morphology	
	Wt. avg. T_c (°C)[a]	$\Delta H_{c,hom}$ (J/g POM)	$\Delta H_{c,114\,°C}$ (J/g POM)	$\Delta H_{c,127\,°C}$ (J/g POM)	$\Delta H_{c,bulk}$ (J/g POM)	$X_{c,DSC}$ (%)	$X_{c,WAXD}$ (%)	Diameter (μm)	Morphology
POM	146	0	0	0	−168	54	55	–	–
POM/Ha4									
40/60	107	−76	−43	−20	0	47	52	1.8	Droplets
30/70	97	−103	−14	0	0	41	44	1.5	Droplets
20/80	94	−118	0	0	0	41	40	1.2	Droplets
10/90	94	−118	0	0	0	41	33	1.0	Droplets
5/95	94	−115	0	0	0	40	25	0.7	Droplets
POM/Ha7									
40/60	142	−9	0	0	−126	44	55	0.8	Co + sub[b]
30/70	128	−40	0	0	−85	41	55	0.8	Co + sub[b]
20/80	107	−79	−10	0	−30	40	40	0.6	Droplets
10/90	91	−117	0	0	0	41	33	0.5	Droplets
5/95	91	−112	0	0	0	39	23	0.3	Droplets

[a] A weight average crystallization temperature is calculated on the basis of T_c and X_c values determined by DSC: Wt. avg. $T_c = (X_{c,hom} \times T_{c,hom}) + (X_{c,114\,°C} \times T_{c,114\,°C}) + (X_{c,127\,°C} \times T_{c,127\,°C}) + (X_{c,bulk} \times T_{c,bulk})$.
[b] Composite phase morphology of co-continuous POM and PS/PPE phases together with very small subinclusions of POM in the PS/PPE domains.

decreasing droplet diameter has an impact on the parameters governing the degree of crystallinity. Note, however, that $X_{c,DSC}$ comprises all heat released during crystallization, while $X_{c,WAXD}$ reflects only the amount of crystalline POM that is sufficiently ordered to give rise to reflections [49].

The relative crystallite sizes were calculated from the full width at half-maximum of the reflections using Eq. (1). The (100) reflection corresponds to lattice planes parallel to the molecular chain axes. The width of this peak is thus a measure for the size L_1 of the crystallites in a direction perpendicular to the molecular axes, i.e. it is a measure for the square root of the number of chains passing through a crystallite [50]. The width of the (105) reflection is a measure for the size L_2 of the crystallites parallel to the molecular axes, since the perpendicular to the (105) plane is inclined at an angle of 41.8° to the molecular chain axes [50]. The evolution of the crystallite sizes L_1 and L_2 as a function of POM content in the blends is displayed in Fig. 6.

The evolution of the crystallite sizes, L_1 and L_2, as a function of the POM content in the blends parallels that of $X_{c,WAXD}$. Blends in which the POM phase is predominantly crystallized by heterogeneous nucleation at low degrees of undercooling (e.g. POM/Ha7 40/60) have the same value for X_c, L_1 and L_2 as the POM homopolymer ($X_c \approx 55\%$, $L_1 \approx 110$ Å and $L_2 \approx 90$ Å). As soon as homogeneous crystallization dominates (i.e. more than 50% of the POM phase crystallizes at $T_{c,hom}$), the crystal size gradually decreases until it reaches $L_1 = 95$ Å and $L_2 = 64$ Å. The crystal sizes correlates better with the amount of fractionated crystallization rather than with the degree of crystallinity. The correlation between the crystal sizes, $X_{c,WAXD}$ and the overall blend phase morphology is presented in Fig. 7.

There is a strong correlation between $X_{c,WAXD}$ and the weight average particle diameter in both blend series; smaller particles systematically result in a lower X_c, which as illustrated in Fig. 7b, is not simply related to the drop in crystallization temperature.

The evolution of $X_{c,WAXD}$ as a function of the total number of particles per vol% POM in the blend series reveals that both L_1 and X_c remain constant below a critical number of POM particles. Both X_c and L_1 gradually decrease in dispersions containing more POM particles per vol% POM. The lower value of L_1 indicates that the number of chains passing through the crystallite and the lateral dimensions of the crystallites become smaller. Consequently, there must be a linear relation between the lateral crystallite dimension, L_1, and the final value of

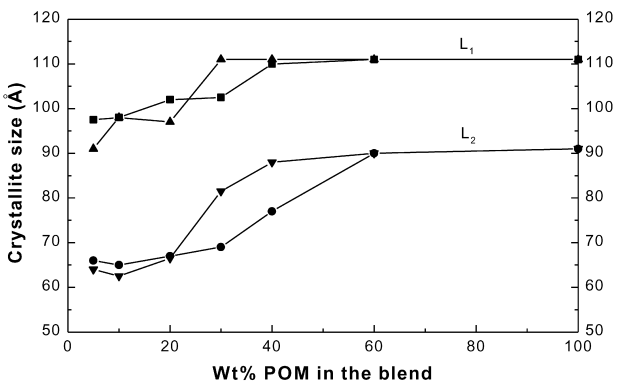

Fig. 6. Influence of the weight percentage POM in POM/(PS/PPE) blends on the relative crystallite sizes, L_1 and L_2, calculated from the peak width at half-height of the crystalline reflections in WAXD. L_1 is calculated from the (100) reflection in POM/Ha4 (■) and POM/Ha7 (▲); L_2 is calculated from the (105) reflection in POM/Ha4 (●) and POM/Ha7 (▼).

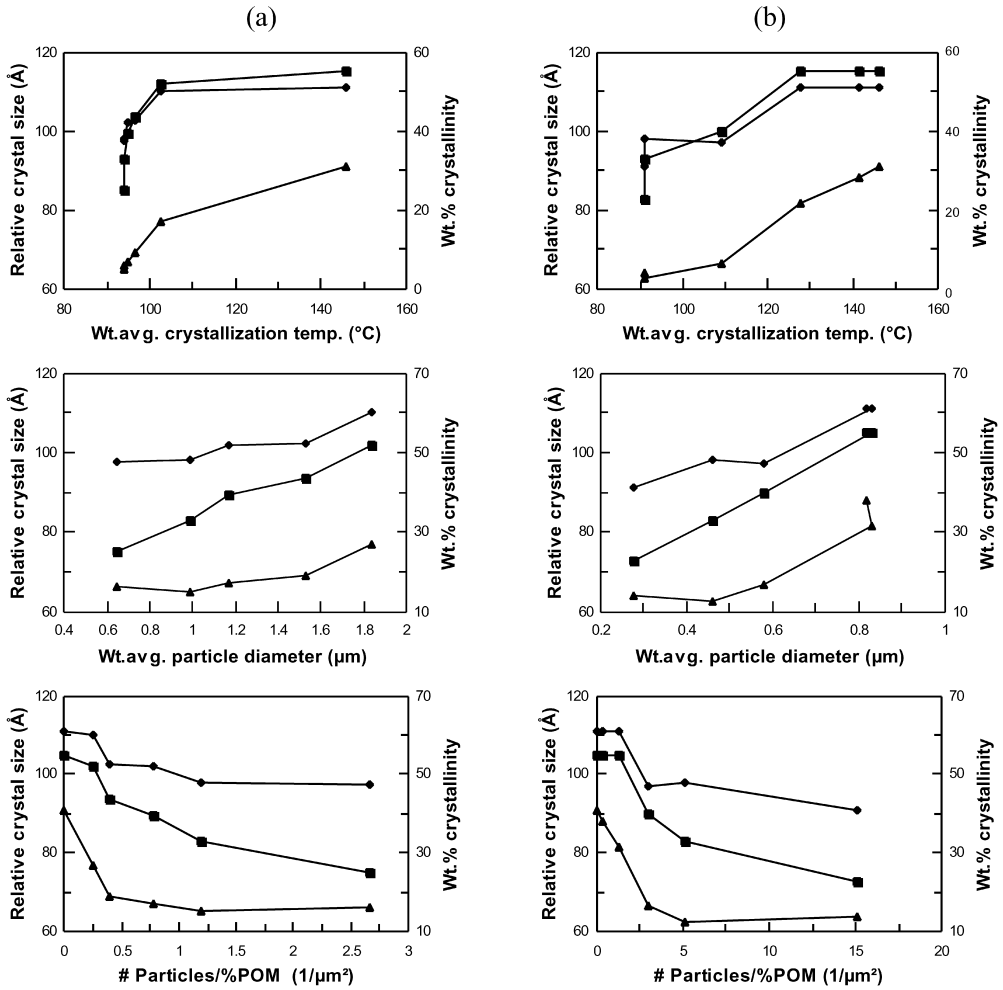

Fig. 7. Correlation of the degree of crystallinity as measured from the crystalline peak area in WAXD (■), and the relative crystal sizes L_1 determined from the (100) reflection (◆) and L_2 determined from the (105) reflection (△) with the weight average crystallization temperature, weight average particle diameter, and number of POM particles per percentage POM in the blend.(a) POM/Ha4 blends; (b) POM/Ha7 blends.

$X_{c,WAXD}$, independently of the blend series, crystallization temperature or phase morphology as illustrated in Fig. 8a. This also clarifies the relationship between $X_{c,WAXD}$ and the droplet size; smaller droplets having a profound influence on the lateral dimensions of the crystalline lamellae. Smaller lateral dimensions imply a loss of the fraction of crystallizable POM in the droplets, which lowers X_c. There is no such linear relationship with the crystal size, L_2, which is a measure of the lamellar thickness of the crystals (Fig. 8b), suggesting that lower value of X_c cannot solely be attributed to a reduction of the lamellar thickness. Note that the relationships between X_c and L_2 are identical for both blend series (Fig. 8).

The correlation between $X_{c,WAXD}$, L_1 and the droplet size provides a possible explanation for the discrepancy between the evolution of $X_{c,DSC}$ and $X_{c,WAXD}$ as a function of the weight percentage POM in the blends. In polyethylenes, imperfect crystallites give a diffuse halo rather than sharp reflections in WAXD [49]. By analogy, the difference between $X_{c,WAXD}$ and $X_{c,DSC}$ can be attributed to an increasing amount of small, very imperfect crystals and the lower $X_{c,WAXD}$-values associated with lower droplet sizes suggest that small imperfect crystallites mainly form when the mobility of the polymer chains is restricted and the high degree of undercooling requires much smaller critical nucleus dimensions. Furthermore, homogeneous crystallization of PE dispersed in droplets proceeds in a nucleation mode, in which the nucleation rate is so high that there is a lack of space for lateral growth, leading to the formation of small and highly imperfect crystalline structures [44]. A similar behavior is reported for low density homogeneous ethene-1-octene copolymers with high degrees of comonomer [51], where the restricted mobility of the crystallizable chain and the lower crystallization temperature leads to the formation of small crystallites which can no longer be detected by WAXD.

3.3. Static small angle X-ray scattering measurements

Static SAXS measurements were performed at room temperature on dynamically crystallized POM/(PS/PPE) blends to study the influence of fractionated crystallization

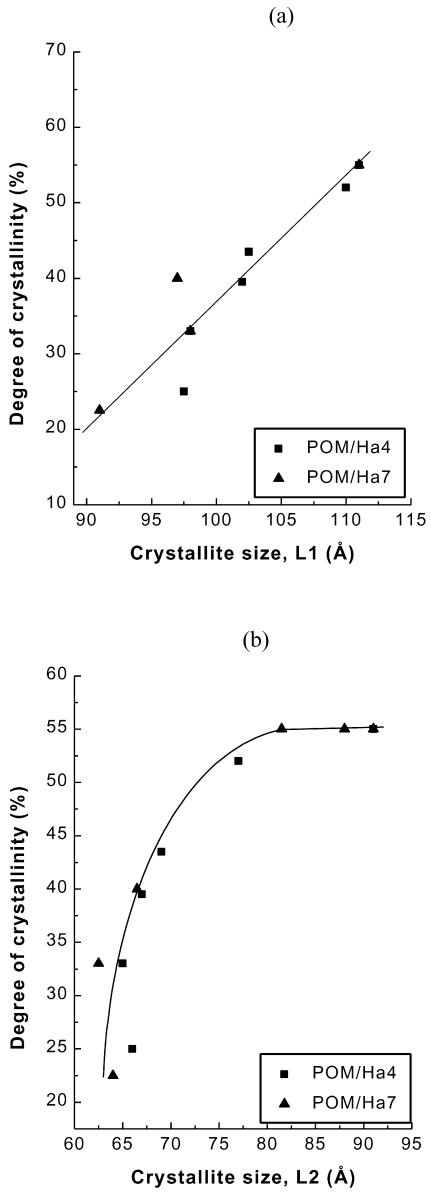

Fig. 8. Correlation between the relative crystal sizes L_1 (a) and L_2 (b) calculated from WAXD and the total degree of crystallinity as measured from WAXD.

on the semicrystalline structure. Several parameters, such as high crystallization rates due to higher degrees of undercooling, spatial restrictions in small droplets, homogeneous nucleation mechanism, etc. can directly affect the semicrystalline structure.

The long period, $\langle L \rangle_w$, is determined from the position of the maximum of Lorentz-corrected SAXS curves assuming the existence of parallel crystalline lamellae [52,53] as found in most polymers of medium to high crystallinity, such as POM. Since the POM/(PS/PPE) blends are completely immiscible, the POM domains are not diluted by the amorphous PS/PPE phase and thus not expected to form more or less isolated lamellae, as seen in highly diluted miscible blend systems [54]. No indications were found in the literature suggesting the existence of such isolated lamellae in POM crystallized at $T_{c,hom}$ and no evidence for a non-lamellar semicrystalline structures was found in any of the present blends.

Hoffman and Weeks [55] reported that extremely small folded chain crystals form in a spherulitic superstructure during homogeneous crystallization of polychlorotrifluoroethylene and attributed this to catastrophic nucleation in homogeneously crystallizing materials. This supports the validity of our assumption of rather parallel lamellae in homogeneously crystallized POM samples. Homogeneous crystallization of polyethylene droplets also resulted in a clear lamellar folded chain morphology with an unusually thick amorphous layer as observed in TEM micrographs [44]. Small isolated lamellae were only observed at the edge of the droplets.

The Lorentz-corrected SAXS curves obtained after dynamic crystallization from the melt and the corresponding long period, $\langle L \rangle_w$, as a function of the weight percentage POM in the blends are shown in Fig. 9.

The overall picture is similar to that observed for the evolution of the crystallite size parallel to the molecular axis, L_2, in WAXD (Fig. 6), suggesting that this could be a good measure for the influence of fractionated crystallization on the lamellar thickness or the long period. The long period remains constant at $\langle L \rangle_w = 150$ Å as long as heterogeneous crystallization at low degrees of undercooling dominates for the majority of the POM droplets.

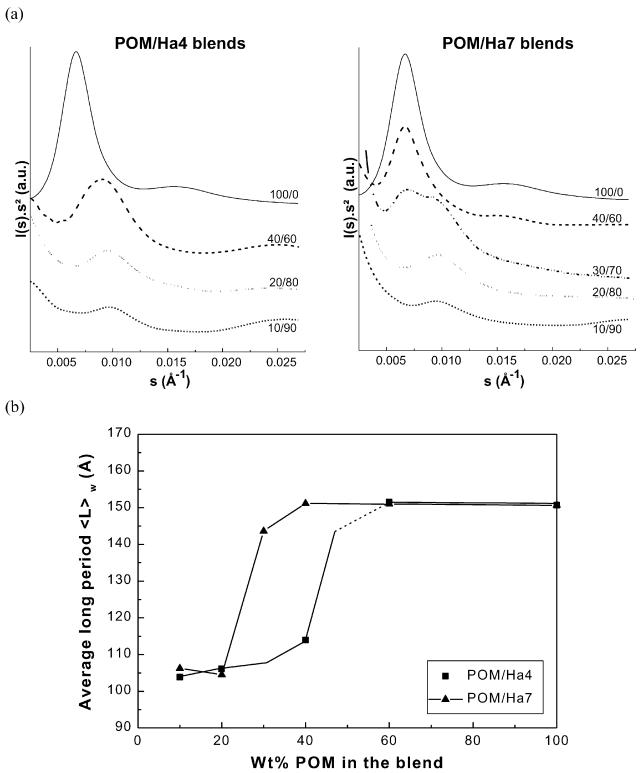

Fig. 9. Influence of the weight percentage POM in POM/Ha4 and POM/Ha7 blends on the semicrystalline morphology, indicated by the average long period calculated from Lorentz-corrected SAXS curves.

Once homogeneous crystallization occurs in a significant fraction of the droplets, the long period gradually decreases and reaches a value of 105 Å in fully homogeneously crystallizing samples. Since the region of phase inversion in POM/Ha7 blends extends up to a 30/70 blend composition and has a typical composite phase morphology, the nearly constant long period up to 30/70 POM/Ha7 must be due to heterogeneously crystallized co-continuous POM domains. Note that the Lorentz-corrected SAXS curve of POM/Ha7 30/70 blends has two maxima. The first one at 144 Å probably corresponds to the average long period in the co-continuous POM domains and the larger droplets crystallized heterogeneously, while the second one at 110 Å can be attributed to the average long period of the fraction of small subinclusions crystallized by homogeneous nucleation at high degrees of undercooling. In all blends, where the POM phase was dispersed in fine droplets which predominantly crystallize in the homogeneous mode, $\langle L\rangle_w$ is 105 Å.

From a 40/60 composition onwards POM/Ha4 blends are dispersed in droplets and there is no bulk crystallization as reflected in the evolution of $\langle L\rangle_w$. As soon as POM is entirely dispersed in droplets crystallizing at higher degrees of undercooling, $\langle L\rangle_w$ significantly decreases and reaches a value close to that of fully homogeneously crystallized samples. The long period observed in POM/(PS/PPE) blends is thus characteristic for the dominant mode of crystallization. It varies between 150 Å for fully bulk crystallized POM and 105 Å for fully homogeneously crystallized POM, independently of the blend phase morphology. The change in the long period is thus not directly related to the continuously decreasing value of $X_{c,WAXD}$ with lower POM contents in the blends. This is illustrated in Fig. 10a where long periods between 135 and 150 Å are found, independently of the blend series, for the same $X_{c,WAXD}$, whereas $X_{c,WAXD}$ further decreases for fully homogeneously crystallizing droplets with a constant $\langle L\rangle_w$ of 105 Å. The correlation between $\langle L\rangle_w$ and $X_{c,DSC}$ is even poorer.

The expected linear relationship between average crystallization temperature and long period was found for both POM/Ha4 blends and POM/Ha7 blends (Fig. 10b).

To monitor the evolution of the lamellar thickness as a function of the wt% POM in the blends and the weight average crystallization temperature, normalized linear correlation functions, $\gamma_1(r)$, were calculated from the SAXS patterns, thereby assuming an isotropic semicrystalline structure [56,57]. The long period, $\langle L\rangle_n$, crystalline layer thickness, L_c, amorphous layer thickness, L_a, and volume degree of crystallinity in the lamellar stacks, ϕ, were extracted from the linear correlation function $\gamma_1(r)$ of the POM homopolymer, POM/Ha4 40/60 and 20/80, and POM/Ha7 40/60 blends. In all other cases, $\gamma_1(r)$ could not be calculated because of a bimodal lamellar distribution (i.e. POM/Ha7 30/70) or because the concentration of crystalline lamellae was too small to detect maxima in the SAXS patterns.

An overview of the correlation functions of POM and the

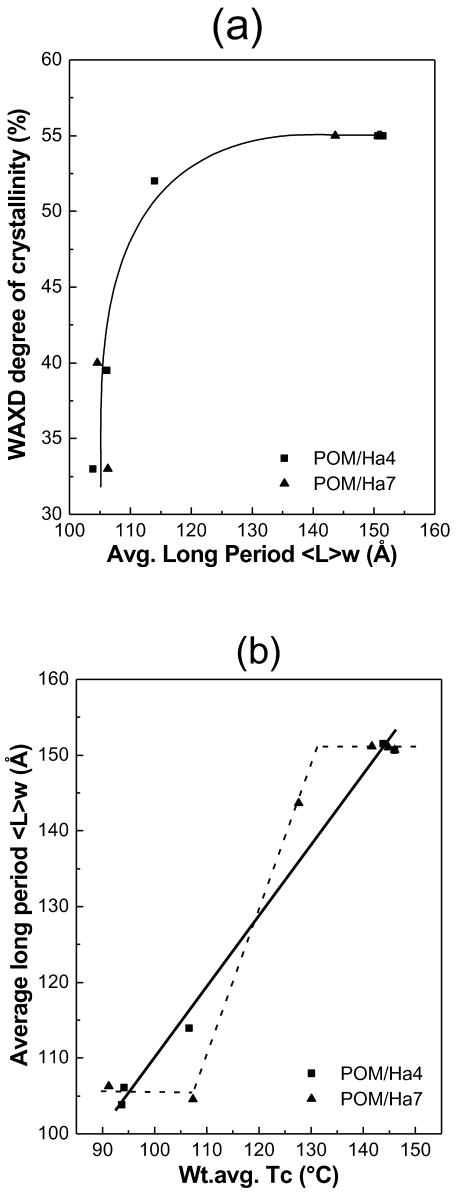

Fig. 10. Correlation of the average long period $\langle L\rangle_w$ calculated from Lorentz-corrected SAXS patterns, with (a) the degree of crystallinity of the POM phase, as determined from WAXD, and (b) the weighted average crystallization temperature of the POM phase.

POM/(PS/PPE) blends, after complete crystallization, is given in Fig. 11. There is a significant change in the long period, $\langle L\rangle_n$ which parallels that of $\langle L\rangle_w$. The lower first maximum in the correlation functions of POM/Ha4 40/60 and especially 20/80 blends compared to that of the POM homopolymer results from distorted lamellar packing and/or broad lamellar thickness distributions [58]. Furthermore, the curvature of $\gamma_1(r)$ near the origin indicates that there is actually a transition layer transition layer between crystalline lamellae and amorphous zones which broadens, as the crystallization shifts from predominantly heterogeneous (i.e. POM, POM/Ha7 40/60) to predominantly homogeneous (i.e. POM/Ha4 40/60 and 20/80). This is related to the higher degrees of undercooling at which

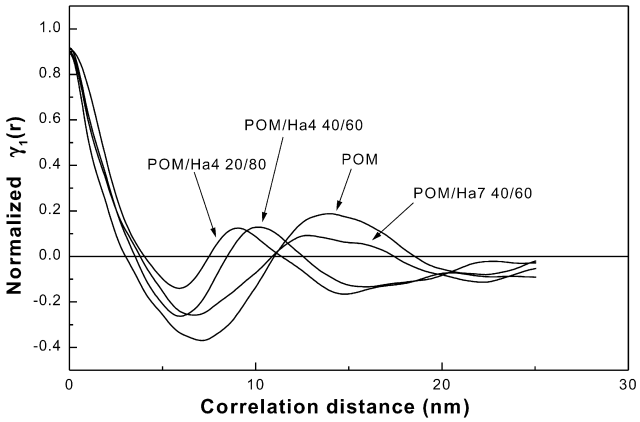

Fig. 11. Overview of the normalized correlation function curves, $\gamma_1(r)$, calculated from SAXS, at room temperature for POM, POM/Ha4 40/60, POM/Ha4 20/80, and POM/Ha7 40/60.

homogeneous crystallization takes place and where faster crystallization kinetics due to higher growth and primary nucleation rates leads to less perfect and/or thinner crystalline lamellae. These results are consistent with the findings of the WAXD analysis.

A detailed list of all parameters calculated from the linear correlation functions is given in Table 3. The macroscopic volume crystallinity, ϕ, was estimated from DSC or WAXD data.

The evolution of the volume degree of crystallinity in the lamellar stacks, and the parameters determining the semicrystalline structure in POM/(PS/PPE) blends as a function of the weight average crystallization temperature of the POM phase are shown in Fig. 12.

These results should be interpreted with caution, since they represent a selection of POM/(PS/PPE) blends, containing sufficiently large amounts of POM to yield a linear correlation function. As the data for POM/Ha4 blends are well spread over the whole temperature region, the trends in Fig. 12 can be considered representative for all blend compositions in this series. Moreover, as illustrated in Fig. 10b, for POM/Ha4 blends the relationship between $\langle L\rangle_w$ and the weight average T_c is linear over the complete crystallization temperature range. Interpretation of the semicrystalline structure in POM/Ha7 blends as a function of crystallization temperature in the low temperature range is uncertain as it relies on a single data point: POM/Ha7 40/

Table 3
Overview of the parameters calculated from SAXS measurements in POM/(PS/PPE) blends

	POM**	POM/Ha4 40/60**	POM/Ha4 20/80*	POM/Ha7 40/60**
Wt. avg. T_c (°C)	146	107	94	142
$\langle L\rangle_n$ (Å)[a]	143	101	94	135
$\langle L\rangle_w$ (Å)[b]	151	114	106	151
$\langle L\rangle_w / \langle L\rangle_n$ [c]	1.05	1.13	1.13	1.12
L_c (Å) cfu[1]	112	59	53	96
DSC[2]	108	59	50	97
WAXD[3]	103	61	48	85
Quadratic equation[4]	119	55	–	101
AVG[5]	112	58	50	95
L_a (Å) cfu[1]	28	40	37	32
DSC[2]	36	42	44	39
WAXD[3]	40	40	46	50
Quadratic equation[4]	25	46	–	34
AVG[5]	30	42	42	37
ϕ (%) cfu[1]	80	59	61	75
DSC[2]	75	59	53	71
WAXD[3]	72	60	51	63
Quadratic equation[4]	83	54	–	75
AVG[5]	79	58	54	72

** Calculated assuming $\phi > 50\%$.
* Quadratic expression could not be calculated since the discriminant is negative; calculated assuming $\phi < 50\%$.
[a] From the center of gravity of the first side maximum in the correlation function.
[b] From the Lorentz-corrected SAXS pattern.
[c] Value indicative for the width of the distribution of periodicities in the stacks.
[1] Determined using the crystallinity, ϕ, from the minimum in the correlation function.
[2] Determined using the volume crystallinity calculated from DSC.
[3] Determined using the volume crystallinity calculated from WAXD.
[4] Determined using the crystallinity obtained via the quadratic equation.
[5] Overall average of all relevant calculations.

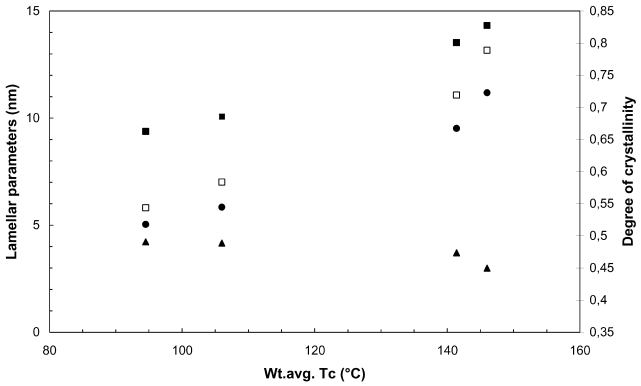

Fig. 12. Evolution of the volume degree of crystallinity in the lamellar stacks, ϕ, and the lamellar parameters calculated from the correlation functions as a function of the weighted average crystallization temperature of the POM phase. Volume degree of crystallinity ϕ (□), long period $\langle L\rangle_n$ (■), amorphous layer thickness L_a (▲), and crystalline lamellae thickness L_c (●).

60, with a weight average T_c of 142 °C. The nature of the heterogeneous nucleation mechanism in finely dispersed POM droplets remainsunclear although nucleation at the solidified Ha7 matrix phase was suggested [25].

For *POM/Ha4 blends*, a decrease in the average crystallization temperature due to a larger fraction of droplets crystallizing homogeneously, results in a drop in crystalline lamellar thickness, L_c, from ±112 Å (POM, $T_c = 146$ °C) to ±50 Å (POM/Ha4 20/80, $T_c = 94$ °C). The average amorphous layer thickness between the crystalline lamellae slightly increases from 30 Å ($T_c = 146$ °C) to 42 Å ($T_c = 94$ °C). Homogeneous crystallization in small droplets hence results in thinner lamellae. The slight increase of L_a may result from progressive broadening of the transition layer between crystalline lamellae and amorphous layers with decreasing crystallization temperature, as a consequence of the formation of less perfect crystalline structures at higher degrees of undercooling. Many studies on polymeric systems reported a decrease in lamellar thickness with an effectively constant amorphous layer thickness. In the present case, this would correspond to a maximum increase of the transition layer thickness of 12 Å (Fig. 13), which is also in agreement with the lower scattering

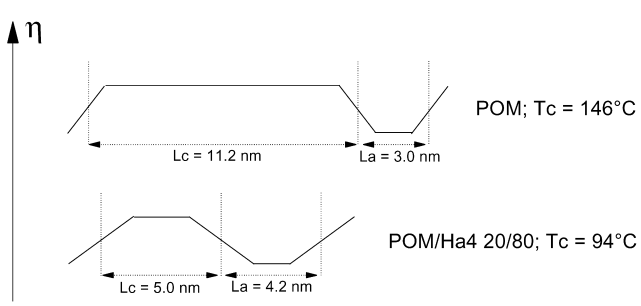

Fig. 13. Schematical representation of the influence of blending minor amounts of POM in a Ha4 matrix on the final semicrystalline morphology of the POM phase. A significant reduction in the crystalline lamellae thickness and a serious broadening of the transition layer between crystalline and amorphous layers is suggested.

intensity of the predominantly homogeneously crystallized samples mentioned above. The drop in volume degree of crystallinity (Φ) in the lamellar stacks from about 80% in the POM homopolymer to about 50% in a POM/Ha4 20/80 blend also indicates the formation of less perfect lamellae. The ratio $\langle L\rangle_w/\langle L\rangle_n$ which is a measure for the polydispersity of the periodicity in the lamellar stacks, also increases in the blends.

The influence of fractionated crystallization on the semicrystalline structure in *POM/Ha7 blends*, can only be interpreted in the region of phase inversion. Surprisingly, the Lorentz-corrected long period, $\langle L\rangle_w$, does not change, although some subinclusions crystallize homogeneously. The long period calculated from the correlation function which is more sensitive gives $\langle L\rangle_n = 135$ Å compared to $\langle L\rangle_n = 143$ Å in the POM homopolymer, in agreement with the decrease of the weight average crystallization temperature. The broad distribution of periodicities in the stacks is also a consequence of averaging the higher long periods in the heterogeneously crystallized co-continuous POM phase and the smaller ones formed in the homogeneously crystallized POM subinclusions. The average crystalline layer thickness drops from 112 Å (POM homopolymer, $T_c = 146$ °C) to 95 Å ($T_c = 142$ °C), while the amorphous layer thickness increases from 30 Å (POM) to 37 Å. Accordingly, the volume degree of crystallinity drops from about 80% in the POM homopolymer to about 72% in the POM/Ha7 40/60 blend.

3.4. Real-time SAXS–WAXD–DSC

Evaluation of the overall degree of crystallinity and the semicrystalline structure (i.e. long spacing, lamellar thickness, crystallinity in the lamellar stacks, etc.) in POM/-(PS/PPE) blends at room temperature clearly demonstrated that these parameters are highly correlated with the weight average crystallization temperature calculated from DSC traces. Note that these parameters are an average over a range of semicrystalline structures formed in different POM volumes each having their own crystallization temperature and spherulite growth rate, where the size of the dispersed volume also plays a role. Moreover, each crystalline structure is subject to thermal shrinkage during further cooling.

The present study aims at establishing the type of semicrystalline structure formed at each of the four fractionated crystallization steps, to allow its identification from DSC traces. This requires real-time monitoring of the different parameters above.

Real-time SAXS–WAXD measurements were performed on the POM homopolymer, POM/Ha4 40/60, 20/80 and 10/90 blends, and POM/Ha7 40/60 and 10/90 blends. The evolution of $\langle L\rangle_w$ and of the invariant, Q, were calculated from the Lorentz-corrected SAXS patterns as a function of temperature and a relative crystallinity index was calculated from the area under the (100) reflection.

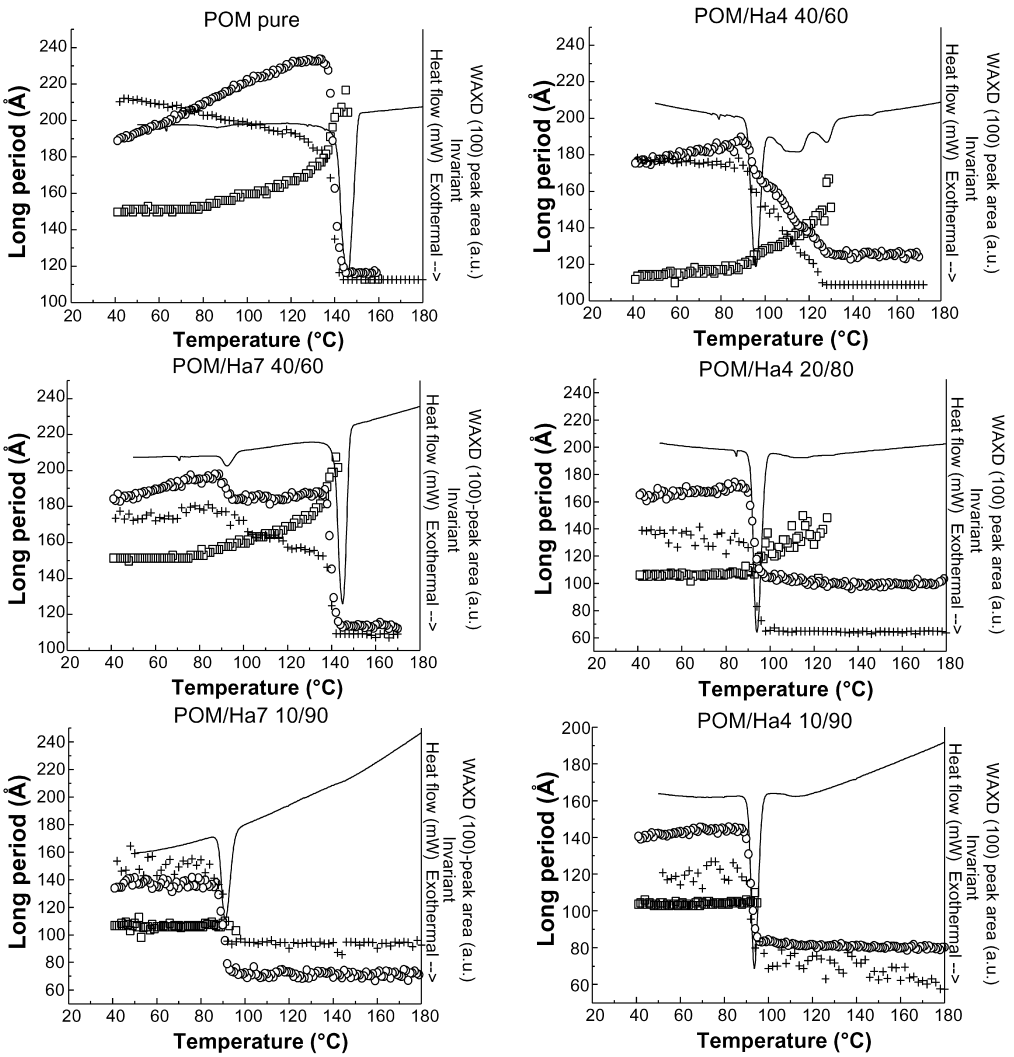

Fig. 14. Overview of the real-time DSC signal (full line), SAXS invariant Q (○), Lorentz-corrected long period $\langle L \rangle_w$ (□), and the WAXD (100) integrated peak area (+) during dynamic crystallization of the POM homopolymer and POM/(PS/PPE) blend systems.

Overview plots of the combined results of DSC, SAXS and WAXD during dynamic crystallization from the melt are shown in Fig. 14.

The results of the three techniques are strongly correlated. The evolution of the SAXS invariant parallels that of the different DSC-exotherms. The relative height of the stepwise increase of the SAXS invariant at each crystallization step also corresponds fairly well with the relative percentage of crystallinity determined by integration of the DSC thermograms (Table 4). Furthermore, the combination of SAXS, WAXD and DSC allows to distinguish more clearly between a small glass transition or a small crystallization exotherm in the DSC trace.

Table 4
Comparison of the relative fractions of POM crystallizing at each crystallization temperature, determined from DSC thermograms and the SAXS invariant

	$T_c = 145$ °C	$T_c = 127$ °C	$T_c = 114$ °C	$T_c = 94$ °C
POM	100[a]/100[b]	−/−	−/−	−/−
POM/Ha4 40/60	−/−	15/23	31/32	55/44
POM/Ha4 20/80	−/−	−/−	6/7	94/93
POM/Ha4 10/90	−/−	−/−	−/4	100/96
POM/Ha7 40/60	90/83	−/−	−/−	10/17
POM/Ha7 10/90	−/−	−/−	−/−	100/100

[a] Relative percentage of the total amount crystallizing POM as determined from DSC thermograms.
[b] Relative percentage of the total amount crystallizing POM as determined from the relative height of the step in the SAXS invariant.

The integrated intensity of the (100) reflection is more scattered but correlates well with the DSC and SAXS results. As demonstrated for POM/Ha4 20/80 blends, WAXD is less sensitive to small amounts of crystalline material than DSC or SAXS. The signal corresponding to the broad DSC-exotherm around 100–120 °C is also detected in the SAXS invariant and there is a maximum in Lorentz-corrected SAXS curves although the WAXD peak area does not change.

The POM homopolymer displays a main bulk nucleated crystallization exotherm at 146 °C, followed by a continu-

ous increase in the degree of crystallinity, integrated WAXD peak area and SAXS invariant during further cooling to room temperature. There is a broad exotherm with a maximum around 87 °C in the DSC trace which should not be confused with the homogeneous crystallization exotherm around 91 °C observed during fractionated crystallization of POM droplets. The POM homopolymer used here is a commercial polymer stabilized against thermal degradation ('unzipping') by copolymerisation with less than 5 wt% ethylene oxide units. Chain segments containing such defects are most probably not readily incorporated in the crystal lattice during primary crystallization and are left to gradually crystallize upon further cooling (secondary crystallization). The linear correlation function analysis of POM during dynamic crystallization from the melt (Fig. 15a) indeed reveals a broad region (100–70 °C) with midpoint around 87 °C where $\langle L\rangle_n$ slightly decreases, but the average thickness of the crystalline lamellae increases and that of the amorphous layer decreases (Fig. 15b). Furthermore, this exotherm is associated with an increase in the volume degree of crystallinity in the lamellar stacks, ϕ, from about 0.7 to 0.8 (Fig. 15c).

The crystallization observed at these low temperatures apparently corresponds to lamellar thickening. Such a broad low temperature exotherm was only observed in fully bulk crystallizing POM samples. In the blend series, the POM phase is generally partly dispersed in fine droplets that crystallize mainly homogeneously giving rise to an exotherm around 91 °C, which may mask the weak signal at 87 °C. The fact that the integrated WAXD intensity curves (I_{WAXD}) of all samples remain constant after the last crystallization step, except for the POM homopolymer, also indicates that there is no secondary crystallization in blends where the POM phase is the minor component.

The POM/Ha4 and POM/Ha7 blends typically crystallize by multiple fractionated crystallization. The long period, $\langle L\rangle_w$, decreases continuously rather than in steps after each additional crystallization step at higher degrees of undercooling, confirming that the semicrystalline structure in each droplet crystallizing at lower temperatures indeed consists of thinner lamellae. The resulting average over all long spacings thus gradually decreases after each crystallization step.

$$O_s = \frac{2\phi}{\langle L_c\rangle_n} \approx \frac{2}{\langle L\rangle_n} \tag{2}$$

Fig. 16 gives an overview of the evolution as a function of temperature of the long periods, $\langle L\rangle_n$ and $\langle L\rangle_w$ in POM/(PS/PPE) blends during dynamic crystallization from the melt.

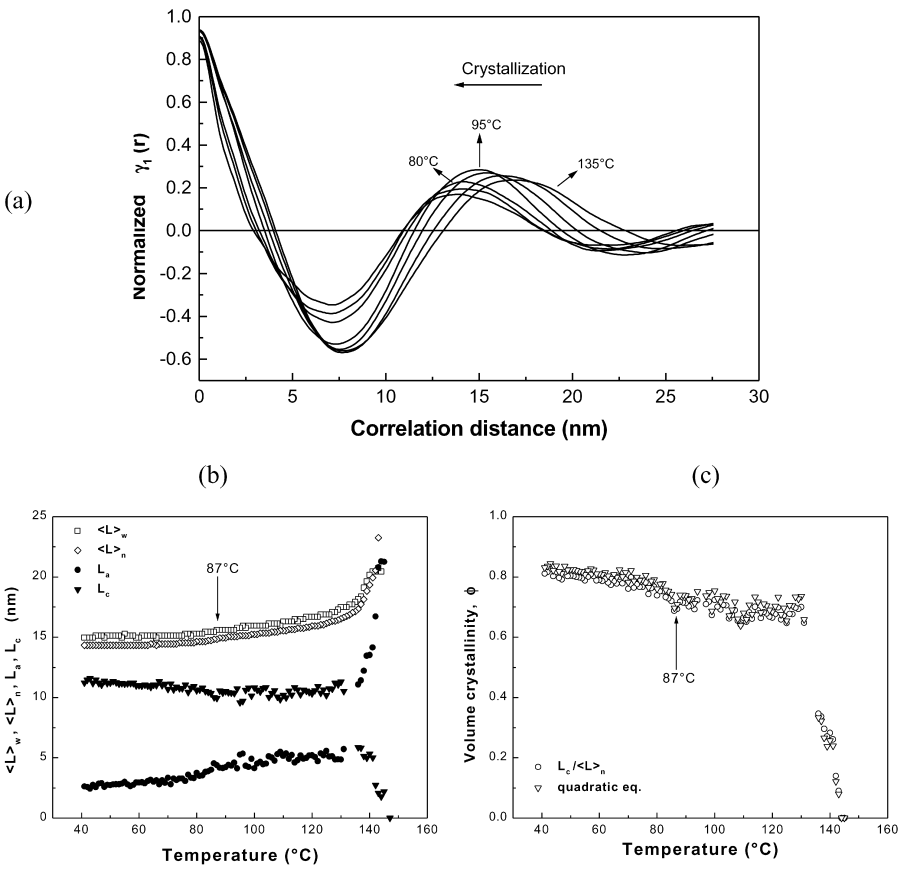

Fig. 15. Real-time SAXS during the crystallization of the POM homopolymer. Evolution of (a) the one-dimensional correlation functions, $\gamma_1(r)$, (b) the long period, amorphous and crystalline layer thickness, and (c) the volume degree of crystallinity in the lamellar stacks, ϕ, as a function of temperature.

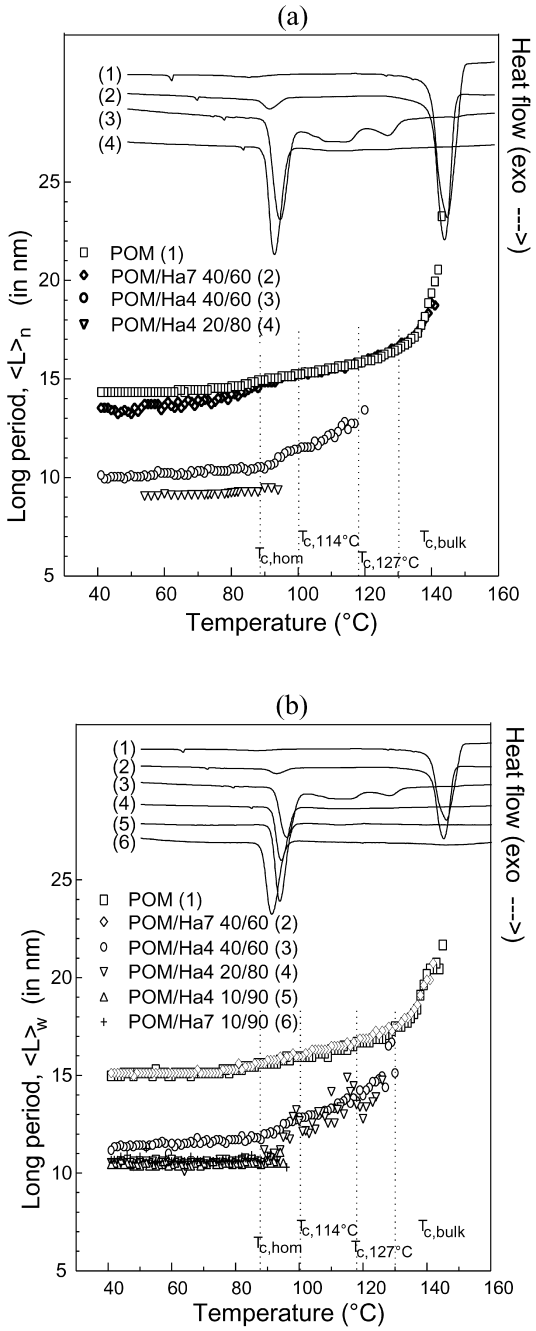

Fig. 16. Influence of the crystallization temperature on (a) the average long period as determined from one-dimensional correlation functions, and (b) the average Lorentz-corrected long period. The first crystallization peak during cooling from the melt always corresponds to a long period of the same size as obtained in other samples crystallizing at the same temperature. Subsequent crystallization peaks lead to a stepwise lowering of the average long period in the sample.

POM droplets crystallizing at the same degree of undercooling have identical long periods as illustrated by the values of $\langle L\rangle_w$ for POM/Ha4 40/60 and 20/80 blends above 100 °C. Once an additional fraction of droplets starts to crystallize at a higher degree of undercooling (i.e. at $T_{c,hom}$), $\langle L\rangle_w$ changes and its final value depends on the amount of additionally crystallized POM. Another effect is observed in the evolution of $\langle L\rangle_n$ in POM and POM/Ha7 40/60 blends. Because the co-continuous POM phase in POM/Ha7 blends crystallizes at $T_{c,bulk}$, both systems have an identical lamellar morphology as long as there is no additional crystallization. Once the POM subinclusions in POM/ha7 40/60 start to crystallize at the homogeneous nucleation temperature (91 °C), the newly formed thinner lamellae in the subinclusions lower the average long period $\langle L\rangle_n$, compared to the POM homopolymer. The final value of $\langle L\rangle_n$ at room temperature indeed differs from that of the POM homopolymer. Note that this is not detected in the evolution of $\langle L\rangle_w$, which is insensitive to this small fraction (in weight) of additional thin lamellae. In contrast, $\langle L\rangle_n$ is proportional to the total surface area of the lamellae, O_s (Eq. (2)) and formation of numerous small lamellae at higher degrees of undercooling increases the total lamellar surface area leading to a significant decrease in $\langle L\rangle_n$.

Because each crystallization temperature seems to be associated with one semicrystalline structure defined by its long spacing and lamellar thickness, calculations were performed to estimate the long spacing expected at temperatures between $T_{c,bulk}$ and $T_{c,hom}$. Table 5 gives an overview of both $\langle L\rangle_w$ and $\langle L\rangle_n$, after each of the four crystallization steps.

The actual long period in the droplets immediately after completion of crystallization at T_c can be estimated from the known weight percentage POM crystallizing at each step, and the average long period at the end of each crystallization step, as illustrated Fig. 17.

The initial crystal structure may still change upon further cooling due to additional interlamellar crystallization (especially at $T_{c,bulk}$) and shift the curve correlating T_c and $\langle L\rangle$ to somewhat lower values. Crystals formed at higher temperatures are more liable to such sporadic crystallization than homogeneously formed ones, as indicated by the evolution of $\langle L\rangle_w$ as a function of temperature in Fig. 14.

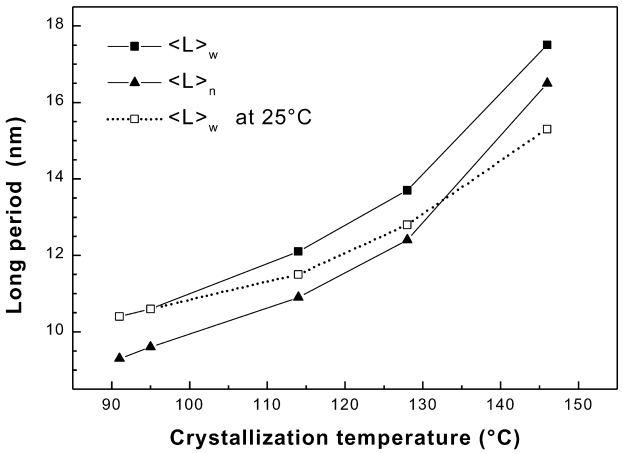

Fig. 17. Influence of the crystallization temperature on the Lorentz-corrected long period $\langle L\rangle_w$ (■) and the long period determined from the one-dimensional correlation function $\langle L\rangle_n$ (△) immediately after the crystallization event, and on the finally obtained Lorentz-corrected long period after cooling to room temperature (□).

Table 5
Overview of the semicrystalline structure (long spacing in Å) in POM/(PS/PPE) blends after each fractionated crystallization step

Sample	Crystallization behavior	After $T_{c,bulk}$ (130 °C)	After $T_{c,127\ °C}$ (116 °C)	After $T_{c,114\ °C}$ (100 °C)	After $T_{c,hom}$ (80 °C)	At T_{room} (40 °C)
POM	T_c = 146 °C; 100%	175[a]/165[b]	164/157	159/152	153/146	150/143
	T_c = 128 °C; 14%	−/−	137/124			
POM/Ha4	T_c = 114 °C; 31%			128/114		
40/60	T_c = 96 °C; 55%				117/104	113/101
POM/Ha4	T_c = 114 °C; 7%	−/−	(135)/ −	120/[c]		
20/80	T_c = 94 °C; 93%				107/93	106/92
POM/Ha4	T_c = 94 °C; 100%				104/[c]	104/[c]
10/90						
POM/Ha7	T_c = 145 °C; 90%	175/166	166/157	160/152		
40/60	T_c = 93 °C; 10%				153/142	151/135
POM/Ha7	T_c = 91 °C; 100%	−/−	−/−	−/−	107/[c]	106/[c]
10/90						

[a] Long period, $\langle L\rangle_w$, determined from Lorentz-corrected SAXS patterns (in Å).
[b] Long period, $\langle L\rangle_n$, determined from the SAXS linear correlation function (in Å).
[c] Correlation function could not be calculated.

The high temperature side of the curve will thus be lowered somewhat more than the low temperature side. It is clear from Fig. 17 that the long period and hence also the lamellar thickness, are directly related to the temperature at which the POM phase crystallized.

In Table 6, the long period of all blends is predicted on the basis of the $\langle L\rangle_w - T_c$ relationship, and the POM fractions crystallizing at each of the four crystallization temperatures, measured by DSC. The values are close to the experimental ones for the POM/Ha4 blends and POM/Ha7 blends crystallizing at a weight average T_c close to $T_{c,bulk}$. The DSC crystallization temperature thus allows to accurately predict the long period formed in the material at each crystallization step. Conversely, the long spacing gives information about the thermal history of the sample. However, note that knowledge of the long period does not give any information about the lateral dimensions of the crystalline lamellae. As demonstrated previously, the degree of crystallinity is not only related to the lamellar thickness but also to the lateral dimensions of the crystallites, which are determined by the droplet size.

4. Conclusions

The semicrystalline structure and degree of crystallinity in fractionated crystallizing POM/(PS/PPE) blends where POM is the minor component have been investigated by combining DSC, SAXS and WAXS, resulting in very consistent results.

DSC revealed a significant decrease in the degree of crystallinity with decreasing contents of POM from about 54% in fully bulk crystallizing POM blends to about 40% in fully homogeneously crystallizing blends.

WAXD indicated that fractionated crystallizing droplets only contain the trigonal form of POM. The degree of

Table 6
Prediction of the long period $\langle L\rangle_w$ at room temperature, from the $\langle L\rangle_w - T_c$ relationship and DSC data

Material	% at				$\langle L\rangle_w$ (25 °C) predicted	$\langle L\rangle_w$ (25 °C) experimental
	$T_{c,hom}$	$T_{c,114\ °CC}$	$T_{c,127\ °C}$	$T_{c,bulk}$		
POM	0	0	0	100	153	151
POM/Ha4						
40/60	55	31	14	0	111	114
30/70	88	12	0	0	106	106
20/80	93	7	0	0	106	−
10/90	100	0	0	0	105	104
POM/Ha7						
40/60	10	0	0	90	148	151
30/70	32	0	0	68	138	144
20/80	67	8	0	25	118	105
10/90	100	0	0	0	105	106

crystallinity calculated from WAXD ($X_{c,WAXD}$) drops as soon as the POM phase is fully dispersed. In finely dispersed blends containing only low concentrations of POM, $X_{c,WAXD}$ further decreased with decreasing contents of POM, whereas $X_{c,DSC}$ remained constant at about 40%. This was attributed to the small and highly imperfect crystalline structures formed during homogeneous crystallization in small droplets, which are not detectable by WAXD.

Analysis of the full width at half-maximum of the WAXD reflections gave a linear correlation between L_1, corresponding to the lateral dimensions of the crystallites, and the particle diameter and degree of crystallinity. L_2, which is a measure of lamellar thickness, is non-linearly correlated with the degree of crystallinity, indicating that the decrease in $X_{c,WAXD}$ cannot be solely attributed to the formation of thinner lamellae at higher degrees of undercooling.

SAXS analysis of the POM/(PS/PPE) blends revealed no direct correlation between the long period and the degree of crystallinity. There is, however, a linear relationship between the decrease in $\langle L \rangle_w$ from 151 Å in fully bulk crystallized POM blends to 105 Å in fully homogeneously crystallizing blends, and that of the crystallization temperature. Fractionated crystallization at higher degrees of undercooling results in thinner and less perfect crystalline lamellae. The crystallization temperature determines the thickness and degree of perfection of the crystalline lamellae. The lateral dimensions of crystallites formed in small droplets are mainly governed by the size of the droplets and the WAXD degree of crystallinity is directly related to the particle diameter.

Acknowledgements

The authors are indebted to the Dow Benelux N.V. company (Terneuzen, NL) for financial support and to Dr L. Aerts for his interest in this work. The European Union is thanked for support of the work at EMBL Hamburg through the HCMP Access to Large Installations Project (Contract number CHGE-CT93-0040). General Electric Plastics (Bergen-op-Zoom, NL) is thanked for supplying the PPE-800 and DSM Research (Geleen, NL) for giving the opportunity of melt-blending the PS/PPE mixtures.

References

[1] Everaert V, Groeninckx G, Aerts L. Polymer 1999;40:6627.
[2] Utracki LA. Polymer alloys and blends. Munich: Hanser Publishers; 1989.
[3] Folkes MJ, Hope PS, editors. Polymer blends and alloys. London: Blackie Academic and Professional; 1993.
[4] Koutsky JA, Walton AG, Baer E. J Appl Phys 1967;38:1832.
[5] Klemmer N, Jungnickel B-J. Colloid Polym Sci 1984;262:381.
[6] Frensch H, Jungnickel B-J. Colloid Polym Sci 1989;267:16.
[7] Frensch H, Harnischfeger P, Jungnickel B-J. In: Utracki L, Weiss RA, editors. Multiphase polymers: blends and ionomers. ACS Symp. Ser., vol. 395.; 1989. p. 101.
[8] Frensch H, Jungnickel B-J. Plast Rubber Compos Process Appl 1991; 16:5.
[9] Tang T, Huang B. J Appl Polym Sci 1994;53:355.
[10] Santana OO, Müller AJ. Polymer Bull 1994;32:471.
[11] Baïltoul M, Saint-Guirons H, Xans P, Monge P. Eur Polym J 1981;17: 1281.
[12] Müller AJ, Arnal ML, Morales RA, Europhysics Conference Abstracts, 19D, P2, Prague, 17–20 July; 1995.
[13] Morales RA, Arnal ML, Müller AJ. Polymer Bull 1995;35:379.
[14] Ghijsels A, Groesbeek N, Yip CW. Polymer 1982;23:1913.
[15] O'Malley JJ, Crystal RG, Erhardt PF. ACS Div Polym Chem Polym Prepr 1969;10:796.
[16] Tang T, Huang B. J Polym Sci Polym Phys Ed 1994;B32:1991.
[17] Ikkala OT, Holsti-Miettinen RM, Seppälä J. J Appl Polym Sci 1993; 49:1165.
[18] Moon H-S, Ryoo B-K, Park J-K. J Polym Sci Polym Phys Ed 1994; B32:1427.
[19] Vonnegut BJ. J Colloid Sci 1948;3:563.
[20] Aref-Azar A, Hay J, Marsden B, Walker N. J Polym Sci Polym Phys Ed 1980;B18:637.
[21] Lotz B, Kovacs AJ. ACS Div Polym Chem Polym Prepr 1969;10:820.
[22] Robitaille C, Prud'homme J. Macromolecules 1983;16:665.
[23] Seow PK, Gallot Y, Skoulios A. Makromol Chem 1976;177:177.
[24] O'Kane WJ, Young RJ, Ryan AJ. Macromol Sci Phys Ed 1995;B34: 427.
[25] Everaert V, Groeninckx G, Aerts L. Polymer 2000;41:1409–28.
[26] Schultz AR, Gendron BM. J Appl Polym Sci 1972;16:461.
[27] Prest WM, Porter RS. J Polym Sci Polym Phys 1972;10:1639.
[28] Everaert V, Groeninckx G, Aerts L, Pionteck J, Favis B, Moldenaers P, Mewis J. Polymer 2000;41:1011–25.
[29] Rabiej S. Eur Polym J 1991;27:947.
[30] Young RJ, Lovell PA, Introduction to polymers, London: Chapman and Hall; 1991.
[31] Ryan AJ, Bras W, Mant GR, Derbyshire GE. Polymer 1994;35:4537.
[32] Scherrer P. Gött Nachr 1918;2:98.
[33] Klug HP, Alexander LE, editors. X-ray diffraction procedures for polycrystalline and amorphous materials. New York: Wiley; 1974. Chapter 9.
[34] Koch MHJ, Bordas J. Nucl Instrum Methods 1983;208:461.
[35] Boulin CF, Kempf R, Koch MHJ, McLaughin SM. Nucl Instrum Methods 1986;A249:399.
[36] Boulin CF, Kempf R, Gabriel A, Koch MHJ. Nucl Instrum Methods 1988;A269:312.
[37] Rapp G, Gabriel A, Dosière M, Koch MHJ. Nucl Instrum Methods 1995;A357:178.
[38] Vonk CG, Kortleve G. Kolloid Z Z Polym 1967;220:19.
[39] Strobl GR, Schneider MJ. J Polym Sci Polym Phys Ed 1980;18:1343.
[40] Balta-Calleja FJ, Vonk CG. X-ray scattering of synthetic polymers. Amsterdam: Elsevier; 1989. Chapter 7.
[41] Brandrup J, Immergut EH, editors. Polymer handbook. New York: Wiley; 1989.
[42] Gandica A, Magill JH. Polymer 1972;13:595.
[43] Barham PJ, Chivers RA, Jarvis DA, Martinez-Salazar J, Keller A. J Polym Sci Polym Lett Ed 1981;19:539.
[44] Barham PJ, Jarvis DA, Keller A. J Polym Sci Polym Phys Ed 1982;20: 1733.
[45] Hirami M. J Macromol Sci- Phys 1984;B23:397.
[46] Avrami M. J Chem Phys 1940;8:212.
[47] Billon N, Chanial B, Vivien B, Haudin JM. Ann Chim Fr 1995;20: 355.
[48] Wunderlich B, editor. Macromolecular physics; part 2: crystal nucleation, growth and annealing. New York: Academic Press; 1976.
[49] Aggarwal SL, Tilley GP. J Polym Sci 1955;18:17.
[50] Hammer CF, Koch TA, Whitney JF. J Appl Polym Sci 1959;1:169.
[51] Mathot VBF, Scherrenberg RL, Pijpers TFJ, Engelen YMT. In:

Hosoda S, editor. The new trends in polyolefin science and applications. Research Signpost; 1996.
[52] Crist B. J Polym Sci Polym Phys Ed 1973;11:635.
[53] Crist B, Morosoff N. J Polym Sci Polym Phys Ed 1973;11:1023.
[54] Vonk CG, Pijpers AP. J Polym Sci Polym Phys Ed 1985;23:2517.
[55] Hoffman JD, Weeks JJ. J Chem Phys 1962;37:1723.
[56] Ruland W. Acta Crystallization 1961;14:1180.
[57] Bark M, Zachmann HG. Acta Polym 1993;44:259.
[58] Voigt-Martin IG, Mandelkern L. J Polym Sci Polym Phys Ed 1989;27:967.